

Exploring Halo Substructure with Giant Stars VIII: The Velocity Dispersion Profiles of the Ursa Minor and Draco Dwarf Spheroidals At Large Angular Separations

Ricardo R. Muñoz¹, Peter M. Frinchaboy¹, Steven R. Majewski¹, Jeffrey R. Kuhn²,
 Mei-Yin Chou¹, Christopher Palma³, Sangmo Tony Sohn^{1,4}, Richard J. Patterson¹ &
 Michael H. Siegel^{1,5}

ABSTRACT

We analyze velocity dispersion profiles for the Draco and Ursa Minor (UMi) dwarf spheroidal (dSph) galaxies based on data by Wilkinson et al. (2004) and new Keck HIRES spectra for stars in the outer UMi field. Washington+*DDO*51 filter photometric catalogs provide additional leverage on membership of individual stars, and beyond 0.5 King limiting radii (r_{lim}) identify *bona fide* dSph members five times more efficiently than simple color-magnitude diagram selection schemes. Previously reported “cold populations” at r_{lim} are not obvious in the data and strongly depend on binning: more or less flat and platykurtic dispersion profiles are characteristic of these dSphs at large radii. For either dSph the velocity dispersion of the outermost stars lies within the range of dispersions for stars at other, smaller projected radii. We report discovery of UMi stars to at least $2.7r_{\text{lim}}$ (i.e., $210'$ or 4 kpc). Even with conservative assumptions, a UMi mass of $M > 4.9 \times 10^8 M_{\odot}$ is required to bind these stars, implying an unlikely global mass-to-light ratio of $M/L > 900 (M/L)_{\odot}$. We conclude that we have found stars tidally stripped from UMi.

Subject headings: galaxies: individual (Ursa Minor dwarf spheroidal, Draco dwarf spheroidal) – galaxies: kinematics and dynamics – Local Group

¹Dept. of Astronomy, University of Virginia, Charlottesville, VA 22903-0818 (rrm8f, pmf8b, srm4n, mc6ss, rjp0i@virginia.edu)

²Institute for Astronomy, University of Hawaii, Honolulu HI 96822 (kuhn@ifa.hawaii.edu)

³Dept. of Astronomy & Astrophysics, Penn State, University Park, PA 16802 (cpalma@astro.psu.edu)

⁴Korea Astronomy and Space Science Institute, 61-1 Hwaam-Dong, Yuseong-Gu, Daejeon 305-348 Korea (tonysohn@kasi.re.kr)

⁵University of Texas – McDonald Observatory Austin, TX 78712 (siegel@astro.as.utexas.edu)

1. Introduction

Dwarf spheroidal (dSph) galaxies are claimed to be strongly dark matter (DM) dominated, with global mass-to-light ($[M/L]_{\text{tot}}$) ratios ranging from a few to hundreds in solar units. Spectroscopic databases are now available for some dSphs to their King limiting radii, r_{lim} (Kleyna et al. 2004; Wilkinson et al. 2004, hereafter W04), and beyond (Tolstoy et al. 2004; Westfall et al. 2005; R. Muñoz et al., in preparation, hereafter M05; S. Sohn et al., in preparation, hereafter S05; S. Majewski et al., in preparation), enabling investigation of the kinematics and inferred mass distribution of these galaxies to large radii. Yet, very low stellar densities, particularly at large angular separations, still formidably challenge efficient spectroscopic study of dSphs. The photometric filtering techniques that are the basis of this series of papers successfully overcome this problem and can substantially increase the radial extent of dSph dynamical surveys.

Derived radial velocity (RV) dispersion (σ_v) profiles for dSphs tend to remain rather flat to well past the core radius. Kleyna et al. (2002) attempted to fit the flat Draco (Dra) dSph profile using two-parameter spherical models (Wilkinson et al. 2002) that yield increasing M/L with radius and a net $(M/L)_{\text{tot}}$ of 440 ± 240 . Lokas (2002), applying a constant anisotropy parameter model to the σ_v profiles of the Fornax and Dra dSphs, derived $\sim 10^9 M_\odot$ masses for these systems. Cosmology-dependent studies (Stoehr et al. 2002; Hayashi et al. 2003) based on Λ CDM models interpret the flat σ_v profiles as consistent with massive DM halos surrounding luminous cores. This interpretation helps alleviate the “missing satellites” problem (Kauffmann et al. 1993; Klypin et al. 1999; Moore et al. 1999) endemic to these cosmologies. On the other hand, MW tidal effects on dSphs have been considered (e.g., Hodge & Michie 1969; Kuhn & Miller 1989; Kuhn 1993; Kroupa 1997; Gómez-Flechoso, Fux, & Martinet 1999; Fleck & Kuhn 2003; M05) with predictions of potentially significant unbound stellar populations producing flat/rising dSph σ_v profiles.

W04 and Kleyna et al. (2004) recently reported rather flat or slightly rising σ_v profiles that suddenly decline near the r_{lim} of the Dra, Ursa Minor (UMi) and Sextans dSphs. Such widely separated cold populations in dSphs are of interest because they have been interpreted as signs of *mild* tidal disruption, but more importantly, because they severely mitigate against the idea of extended, tidally heated populations around dSphs (W04). How far dSphs really extend as well as the bound versus unbound nature of putative “extratidal” components remains unanswered. Spectroscopic observation of dSph-associated stars beyond r_{lim} is thus important to confirm the reality of these extended populations and to ascertain their dynamical state.

In this *Letter* the W04 RVs up to r_{lim} for Dra and UMi are combined with new RVs for UMi stars to several r_{lim} to reassess the σ_v profiles. Washington+*DDO51* filter photometric

surveys of both dSphs aid our discrimination of dSph giant star members. We show that: (1) UMi members exist well past r_{lim} (§3). (2) The σ_v ’s of Dra and UMi remain more or less flat to past r_{lim} (§5). (3) The finding of cold populations near r_{lim} of the dSphs depends strongly on how the data are binned, and furthermore, on the rejection of presumed outliers (§5). (4) The Washington+*DDO*51 method is at least 5 times more efficient at finding *bona fide* dSph members than color magnitude diagram (CMD)-selection schemes (§4).

2. Photometric and Spectroscopic Data

Previous contributions in this series (Majewski et al. 2000a; Majewski et al. 2000b; Palma et al. 2003, hereafter P03; Westfall et al. 2005, S05) show that Washington+*DDO*51 photometry is particularly effective at finding rare dSph giant star members against the high Milky Way foreground in the low density wings of the dSph profile (see §4). We use a similar methodology here, where giant star candidates are selected within the two-color diagram (2CD) boundary shown in (Fig. 1). The UMi photometry is from P03 supplemented with Mosaic camera data along the northeast UMi major axis taken with the Mayall 4-meter telescope on UT 2002 May 4-6. The Dra photometry was obtained with the MiniMosaic (MiniMo) camera on the WIYN telescope on UT 2004 March 12-13. MiniMo’s relatively small field of view ($9.2' \times 9.2'$) is not optimal for large area photometric surveys; these data were taken as a backup project when the instrument for our primary observing program failed. As a consequence we only partially surveyed Dra with an 11×1 (from $40'$ East to $67'$ West) strip of MiniMo pointings and a 1×7 strip from the Dra center to $58'$ North.

We have been unable to obtain spectroscopic follow-up of Dra giant candidates identified with our photometry. However, M. Wilkinson graciously provided the W04 RV database for 416 and 266 observed stars in the directions of the Dra and UMi dSphs, respectively. Typical RV errors for these stars are 2.4 (Dra) and 2.9 km s^{-1} (UMi). We cross-identify by celestial coordinates 254 UMi field stars (95%) but only 162 Dra field stars (39%) between the W04 RV and our own photometric databases.

To these data we add Keck HIRES (Vogt et al. 1994) spectra for 52 UMi field stars obtained UT 2002 May 21-22 and UT 2004 May 12-13 (data available from authors). We deliberately targeted UMi giant candidates at large radii. The spectra were reduced using standard IRAF echelle reduction methodology with RVs determined using the `fxcor` package. Our quoted RV errors are determined as in Vogt et al. (1995) with a median of 4.3 km s^{-1} , but are likely double the true errors based on lower dispersions found among 19 multiple measures of six different UMi stars. Moreover, for nine stars measured in common with Armandroff, Olszewski, & Pryor (1995) we obtain a mean difference of 0.3 km s^{-1} with a

dispersion of only 2.9 km s^{-1} . The union of our data with that of W04 yields 309 unique RVs for the UMi field.

3. Revisiting dSph Membership

The Washington+*DDO*51 database can be used not only to select dSph giant star candidates *before* spectroscopy (as we have done for UMi) but for after-the-fact assessment of the likely membership of stars in existing RV catalogues (e.g., W04). Figure 1 shows the CMD and 2CD for both UMi and Dra. Filled/open circles designate RV stars more/less likely to be giants based on positions in the 2CD (with “giants” here adopted as stars bounded by the thin line). The “likely giant stars” tend to lie closer to the red/asymptotic giant branches of their respective dSphs than the “less likely giants” (Fig. 1).

Figure 2 shows RVs for all stars versus elliptical radius, r_e , normalized to $r_{\text{lim}} = 77.9$ for UMi (P03) and 40.1 for Dra (Odenkirchen et al. 2001). An “elliptical radius” corresponds to the semi-major radius of the ellipse centered on the dSph that intersects the position of the star and has the measured ellipticity of the dSph (0.54 for UMi and 0.29 for Dra; from above references). We adopt elliptical rather than circular radii because a dSph’s gravitational potential and tidal boundary are likely to mimic its observed shape (but we revisit circular radii in §5).

The W04 3σ rejection criterion to discriminate likely members (dashed lines in Fig. 2) corresponds to $\pm 39 \text{ km s}^{-1}$ around a mean of -290.8 km s^{-1} for Dra and $\pm 36 \text{ km s}^{-1}$ around a mean of -245.2 km s^{-1} for UMi. Figure 2 shows that by these criteria all but one of our photometric Dra giant candidates have Dra-like RVs, proving the reliability of our photometric discrimination technique. Unfortunately, the majority of Dra RV stars beyond $r_e = 0.4r_{\text{lim}}$ are not present in our photometric catalog, and, among stars not in our catalog, two (open squares in Fig. 2) lie just outside the RV range at $-246.1 \pm 4.6 \text{ km s}^{-1}$ and $-332.03 \pm 4.8 \text{ km s}^{-1}$. These RV uncertainties are within 1σ of the “Dra member” RV limit. While for ~ 200 Dra members one expects only ~ 0.5 outliers at $> 3\sigma$ for a *Gaussian* distribution, the kurtosis excesses (γ_2) of *both* the Dra and UMi RV distributions flatten from near Gaussian ($\gamma_2 = 0$) to $\gamma_2 = -0.8$ and -0.9 , respectively, at $r_e > 0.4r_{\text{lim}}$, so that more *apparent* “outliers” might be expected. Lokas, Mamon, & Prada (2004) also point out that the expected contamination from red Milky Way stars for this sample and at these RVs is negligible (0.07 ± 0.02 expected interlopers). Thus, we consider that these two RV outliers may be Dra members in our σ_v analysis (§5).

In UMi, a larger number of giant candidates than in Dra live clearly outside the RV

criteria (Fig. 2). Because even the faintest stars with RVs have quite small photometric uncertainties (P03), it is not likely that these “false positives” are due to photometric error, but rather represent either field halo giants or metal-poor dwarf stars (having very weak MgB+MgH absorption). It is intriguing that among the “non-UMi” giant candidates there appears to be RV clumpiness, with 9/9/7 stars having $\sigma_v = 9.2 \pm 2.3/9.6 \pm 2.6/16.6 \pm 4.6 \text{ km s}^{-1}$ around $\langle RV \rangle = 6.4/ - 54.8/ - 163.8 \text{ km s}^{-1}$, respectively. These RV clumps of “giant candidates” have σ_v ’s of order those observed in UMi and Dra, as well as in the Sagittarius (Sgr) tidal tails (Majewski et al. 2004) and are reminiscent of foreground halo substructure found in our similar survey of Carina (M05); our giant star identification method may be finding *other* halo substructure in the UMi field. Nevertheless, the majority of stars we photometrically classify as giants do lie inside the W04 “UMi” RV range (see §4). A remaining photometric giant candidate (*triangle*) lies just outside the UMi RV limits but well inside the giant region in the 2CD *and* along the RGB locus for UMi; we strongly suspect this star is a UMi member and include it in our σ_v analysis (§5). In the end, 182 UMi and 210 (208) Dra stars are included in our σ_v profiles (§5).

4. Photometric efficiency

Particularly at large angular radii, the sky density of dSph stars with brightnesses amenable to current spectroscopic capability (i.e., red giants) is swamped by foreground stars. To improve overall efficiency of target selection, various groups (e.g., W04) select dSph targets by position on/near the dSph’s giant branch in the CMD. This typically decreases foreground contamination by an order of magnitude but “false positive” sources still well outnumber dSph stars outside r_{lim} (Majewski et al. 2005; Westfall et al. 2005). However, our Washington+*DDO*51 photometric technique improves sample reliability by an additional order of magnitude over, for example, the W04 CMD selection.

Over all angular separations (to $r_e = 7.7r_{\text{lim}}$ in the case of UMi) our technique yields a dSph member identification efficiency of 87% for UMi and 99% for Dra. Our “false positive” identifications all lie beyond $0.54r_{\text{lim}}$ (we ignore the possibility that their RV clumping is due to wrapped UMi tidal debris arms, as observed in the Sgr system; Majewski et al. 2003). W04’s overall success rate for their CMD-selected candidates, to only $r_e \sim 0.8r_{\text{lim}}$ for UMi and $r_e \sim 1.8r_{\text{lim}}$ for Dra, is 62% and 50%, respectively. Considering targets with $r_e/r_{\text{lim}} > 0.5$, the W04 efficiency drops to 38% (28/73) and 19% (45/239) respectively, whereas our selection method at similar radii still nets an overall efficiency of 77% (23/30) and 92% (11/12). This five times greater member selection efficiency optimizes the exploration of low density dSphs galaxies with valuable 6 to 10-m class telescope time.

5. Velocity Dispersion Profiles and Interpretation

Our σ_v profiles are computed using equal sample-size binning, but similar results are found with equal, linear bin sizes (though some bins are poorly represented in this scheme). To assess the influence of bin size and geometry Figure 3 shows the UMi dispersion profile versus elliptical radii (panel a) and circular radii (panel b) with 17, 12 and 7 members per bin (and the outermost bins accumulating any odd extra star). As expected, profile variability is less pronounced as the number of stars per bin increases. The general UMi trend is an initial decline in σ_v followed by a gentle rise and then a slightly decreasing profile. The sudden decline to a “cold point” reported by W04 appears only in the highest resolution binning that is most susceptible to statistical fluctuations. In addition, the appearance of the cold point is dependent on W04’s use of circular, rather than elliptical, binning (Fig. 3). While larger samples of stars in the outer regions of dSphs would be helpful, UMi seems to share the trend of flat or slowly rising/declining dispersion profiles observed in the outskirts of other dSphs (Mateo 1997, Westfall et al. 2005, S05, M05).

The Dra profiles (Fig. 4) use 21, 16 and 8 stars per bin from upper to lower panel, with solid circles for the 208 star samples. Open symbols show the outer profiles when the outliers marked as squares in Figure 2 are included. Except for a single bin in the lower profile of panel (b), the same general σ_v behavior is seen at large radii as in UMi: a flat (or maybe slowly decreasing) profile (depending on the binning) is observed past r_{lim} . In fact, a χ^2 fit of the σ_v distribution to a constant value for both UMi and Dra shows that there is no evidence that the outermost stars have a dispersion that is statistically different from those of stars at other, smaller projected radii.

Tidal disruption can create an unbound stellar population near a dSph. This seems to be a natural explanation for producing *both* the observed extended stellar distributions *and* flat/rising velocity dispersion profiles in dSphs (Kuhn & Miller 1989; Kroupa 1997; Fleck & Kuhn 2003; M05). While the flat σ_v profiles observed in UMi and Dra have also been modeled by an ad hoc extended DM halo (Kleyna et al. 2002), two additional piece of evidence support the tidal disruption scenario. First, the observed platykurtic velocity distributions at large radii in both UMi and Dra more closely match the flattened RV distributions of unbound dSph stars at large radii in detailed N-body tidal disruption simulations (e.g. M05).

Second, our new Keck RVs have verified the most widely separated member stars for any dSph other than the tidally disrupting Sgr galaxy. Our most separated UMi-field star having a UMi RV is at a linear distance of 238' or 4.8 kpc and near the minor axis; this star’s elliptical radius of $r_e = 6.6r_{\text{lim}}$ implies a major axis radius of 10.4 kpc if the UMi ellipticity is maintained at all radii. Assuming a spherical potential for UMi, the required mass to keep this star bound to the dSph is $M > 3M_{\text{MW}}(r/R_{\text{GC}})^3$, or $7.6 \times 10^8 M_{\odot}$ assuming a Milky

Way mass within the UMi distance ($R_{\text{GC}} = 69$ kpc) of $M_{\text{MW}} = 7.6 \times 10^{11} M_{\odot}$ (Burkert 1997); this translates to $(M/L)_{\text{tot}} > 1,400 (M/L)_{\odot}$ when we adopt $L = 5.4 \times 10^5 L_{\odot}$ (P03). However, if the tidal boundary of UMi is elongated according to its central ellipticity, this star, were it placed at its corresponding major axis radius (i.e., $r = r_e$ or 10.4 kpc), implies an astounding UMi $(M/L)_{\text{tot}} > 14,400 (M/L)_{\odot}$ for UMi.

It might be argued that the latter star is a field halo interloper, since its RV is only ~ 60 km s $^{-1}$ (to the retrograde side) of that expected for a non-rotating halo (assuming a 232 km s $^{-1}$ solar rotation about the Galactic center) and within the σ_v of a hot MW halo (~ 100 km s $^{-1}$; e.g., Sirko et al. 2004). Higher S/N spectroscopy to test this star’s chemical properties would be useful. However, under the above MW dynamics, the second most separated UMi “RV member” — at $210'$ (4 kpc), or $r_e = 2.7r_{\text{lim}}$ along the UMi major axis — is retrograde by ~ 105 km $^{-1}$. A UMi-bound star at this projected radius implies a UMi mass $> 4.9 \times 10^8 M_{\odot}$ or $(M/L)_{\text{tot}} > 900 (M/L)_{\odot}$. Using a similar method to Łokas et al. (2004), we find that the number of expected MW halo giant contaminants plus very metal poor halo dwarfs in the range of RV, color and magnitude of the present UMi survey is ~ 4 for our 12 deg 2 area, under the assumption that we have observed *all* possible targets in the field. Since only about 3.5 deg 2 of our survey is beyond $2r_{\text{lim}}$ and we have only observed 15% of available targets there, the expected contamination rate for two stars is 0.2 stars; thus we regard as very unlikely that both of the outermost UMi RV members are contaminants.

If either of these outer dSph stars are bound, UMi has the largest M/L of any galaxy by yet *another* order of magnitude *or two* than previously suggested. The corresponding physical dimensions of UMi would rival the King profile extent of the Sgr density distribution, of which a significant fraction, however, has been shown must be *unbound* (Majewski et al. 2003). From the extreme physical dimensions implied it is difficult to avoid the conclusion that true extratidal stars have now been identified from the UMi system — results consistent with suggestions of tidal destruction of this dSph by photometric analyses as early as that of Hodge (1964) and more recently by Martínez-Delgado et al. (2001), P03, and Gómez-Flechoso & Martínez-Delgado (2003). The existence of similar photometric and RV trends between UMi and Dra to at least r_{lim} points to a possible tidal disruption scenario for Dra as well (e.g., Smith, Kuhn, & Hawley 1997).

We gratefully acknowledge support by NSF grant AST-0307851, NASA/JPL contract 1228235, the David and Lucile Packard Foundation, Frank Levinson through the Celerity Foundation, and the IfA/UH.

REFERENCES

Armandroff, T. E., Olszewski, E. W., & Pryor, C. 1995, AJ, 110, 2131

Burkert, A. 1997, ApJ, 474, L99

Fleck, J. & Kuhn, J. R. 2003, ApJ, 592, 147

Gómez-Flechoso, M. A., Fux, R., & Martinet, L. 1999, A&A, 347, 77

Gómez-Flechoso, M. Á. & Martínez-Delgado, D. 2003, ApJ, 586, L123

Hayashi, E., Navarro, J. F., Taylor, J. E., Stadel, J., & Quinn, T. 2003, ApJ, 584, 541

Hodge, W. P. 1964, AJ, 69, 438

Hodge, P. W. & R. W. Michie 1969, AJ, 74, 587

Kauffmann, G., White, S. D. M., & Guiderdoni, B. 1993, MNRAS, 261, 201

Kleyna, J. T., Wilkinson, M. I., Evans, N. W., Gilmore, G., & Frayn, C. 2002, MNRAS, 330, 792

Kleyna, J. T., Wilkinson, M. I., Evans, N. W., & Gilmore, G. 2004, MNRAS, 354, L66

Klypin, A., Kravtsov, A. V., Valenzuela, O., & Prada, F. 1999, ApJ, 522, 82

Kroupa, P. 1997, New Astronomy, 2, 139

Kuhn, J. R. & Miller, R. H. 1989, ApJ, 341, 41

Kuhn, J. R. 1993, ApJ, 409, L13

Lokas, E. L., 2002, MNRAS, 333, 697

Lokas, E. L., Mamon, G. A., & Prada, F. 2004, (astro-ph/0411694)

Majewski, S. R., Ostheimer, J. C., Kunkel, W. E., & Patterson, R. J. 2000a, AJ, 120, 2550

Majewski, S. R., Ostheimer, J. C., Patterson, R. J., Kunkel, W. E., Johnston, K. V., & Geisler, D. 2000b, AJ, 119, 760

Majewski, S. R., Skrutskie, M. F., Weinberg, M. D., & Ostheimer, J. C. 2003, ApJ, 599, 1082

Majewski, S. R., et al. 2004, AJ, 128, 245

Majewski, S. R., et al. 2005, AJ, *submitted*

Martínez-Delgado, D., Alonso-García, J., Aparicio, A., & Gómez-Flechoso, M. A. 2001, ApJ, 549, L63

Mateo, M. 1997, ASP Conf. Ser., 116, 259

Moore, B., Ghigna, S., Governato, F., Lake, G., Quinn, T., Stadel, J., & Tozzi, P. 1999, ApJ, 524, L19

Odenkirchen, M. et al. 2001, AJ, 122, 2538

Palma, C., Majewski, S. R., Siegel, M. H., Patterson, R. J., Ostheimer, J. C., & Link, R. 2003, AJ, 125, 1352 (P03)

Sirko, E., et al. 2004, AJ, 127, 914

Smith, H. A., Kuhn, & Hawley, S. L. 1997, ASP Conf. Ser., 127, 163

Stoehr, F., White, S. D. M., Tormen, G., & Springel, V., 2002, MNRAS, 335, L84

Tolstoy el at., 2004, ApJ, 617, L119

Vogt, S. S., et al. 1994, Proc. SPIE, 2198, 362

Vogt, S. S., Mateo, M., Olszewski, E. W., & Keane, M. J. 1995, AJ, 109, 151

Westfall, K. B., Ostheimer, J. C., Frinchaboy, P. M., Patterson, R. J., Majewski, S. R., & Kunkel, W. E. 2005, AJ, *submitted*

Wilkinson, M. I., Kleyna, J. T., Evans, N. W., & Gilmore, G. F. 2002, ApJ, 330, 778

Wilkinson, M. I., Kleyna, J. T., Evans, N. W., Gilmore, G. F., Irwin, M. J., & Grebel, E. K. 2004, ApJ, 611, L21 (W04)

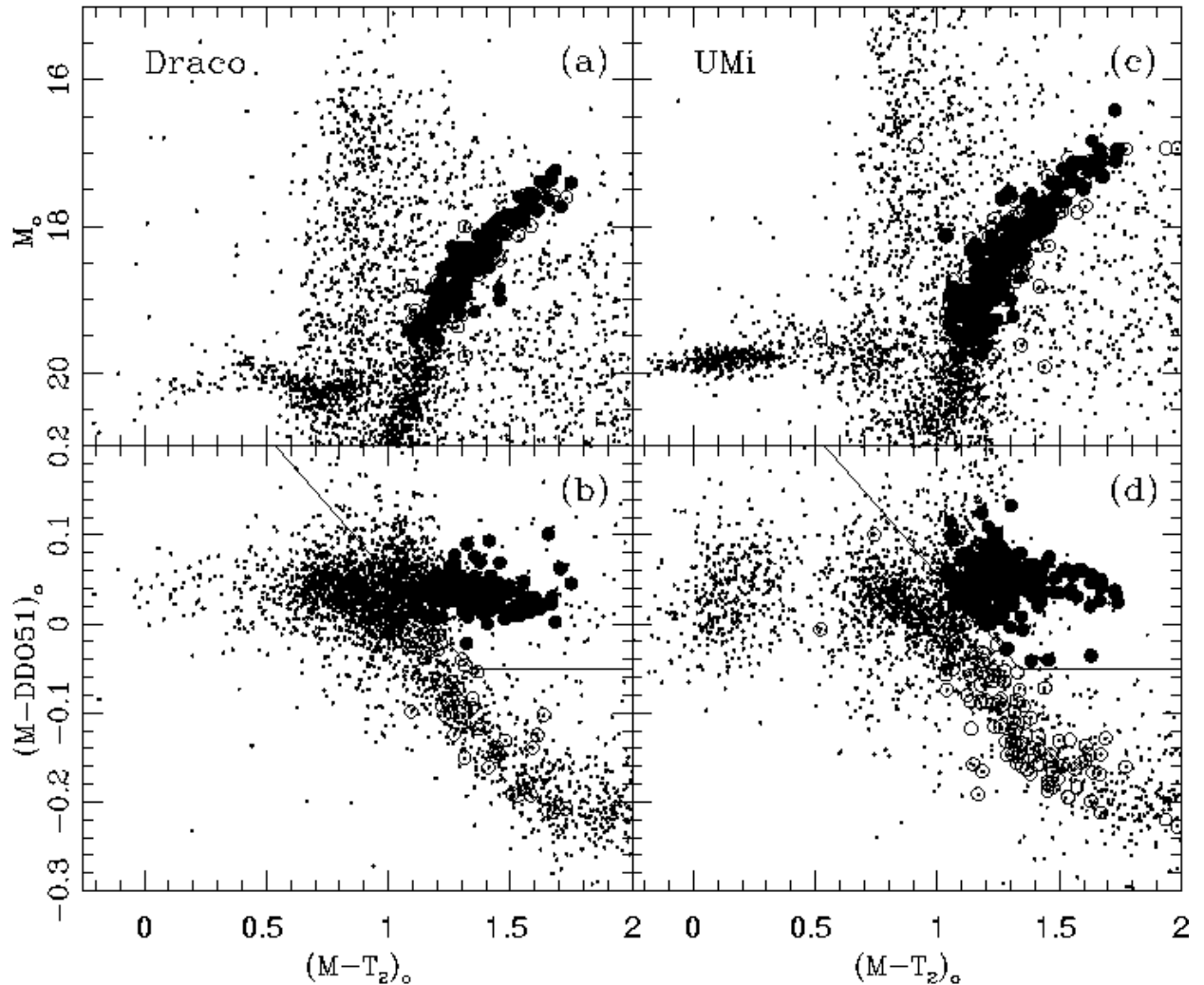


Fig. 1.— (a) Color-magnitude diagram (CMD) for the Dra dSph photometric catalog. Solid/open circles show stars with available RV data selected/not selected photometrically to be Dra giants based on panel (b). (b) $(M - T_2, M - DDO51)_o$ diagram for the same data as panel (a). (c) and (d): CMD and 2CD for the UMi dSph from P03. For clarity, only stars within one r_{lim} have been plotted. Symbols in (c) and (d) have similar meaning as for panels (a) and (b) but for the UMi field.

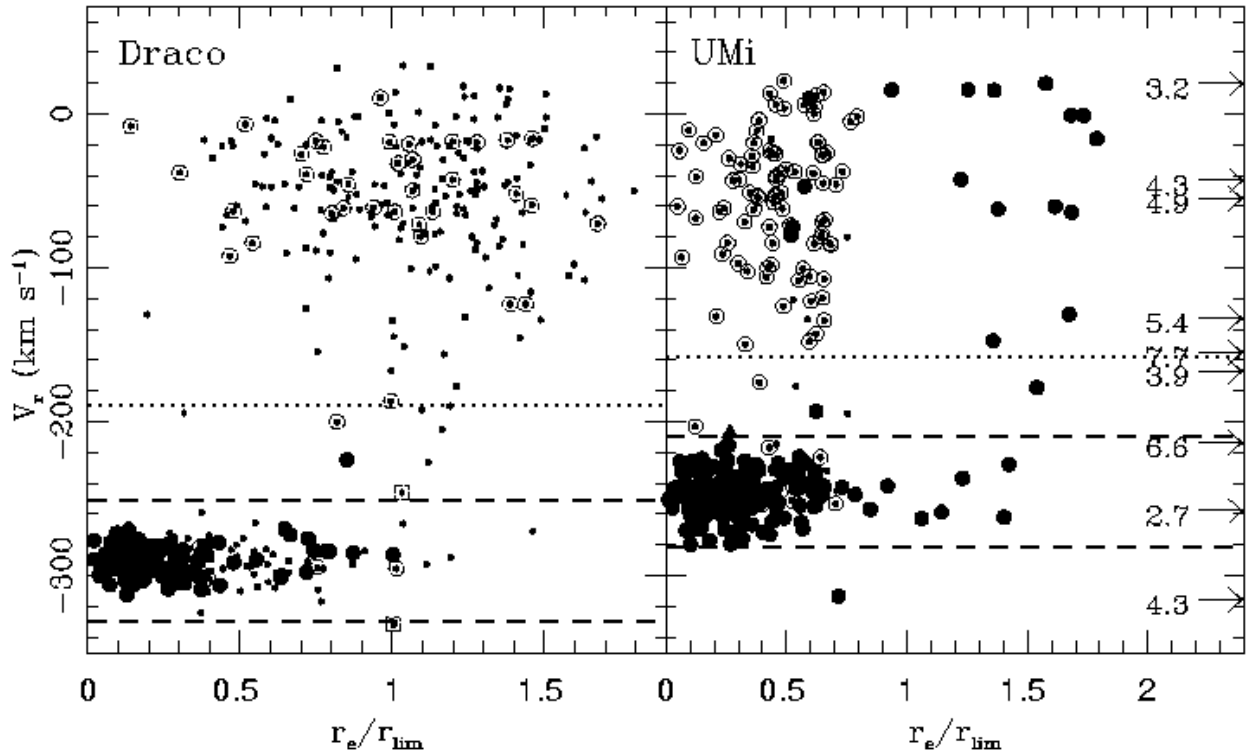


Fig. 2.— RV versus elliptical radius (normalized to r_{lim}) for the Dra (a) and UMi (b) dSphs. Symbols are as in Fig. 1. Dashed lines delineate the 3σ RV range adopted as membership criteria by W04. Arrows indicate the RVs of stars outside the plotted area (normalized radii indicated for these stars by their arrows). Dotted lines show RV expected for zero Galactic rotation velocity, assuming a 232 km s^{-1} solar rotation velocity about the MW.

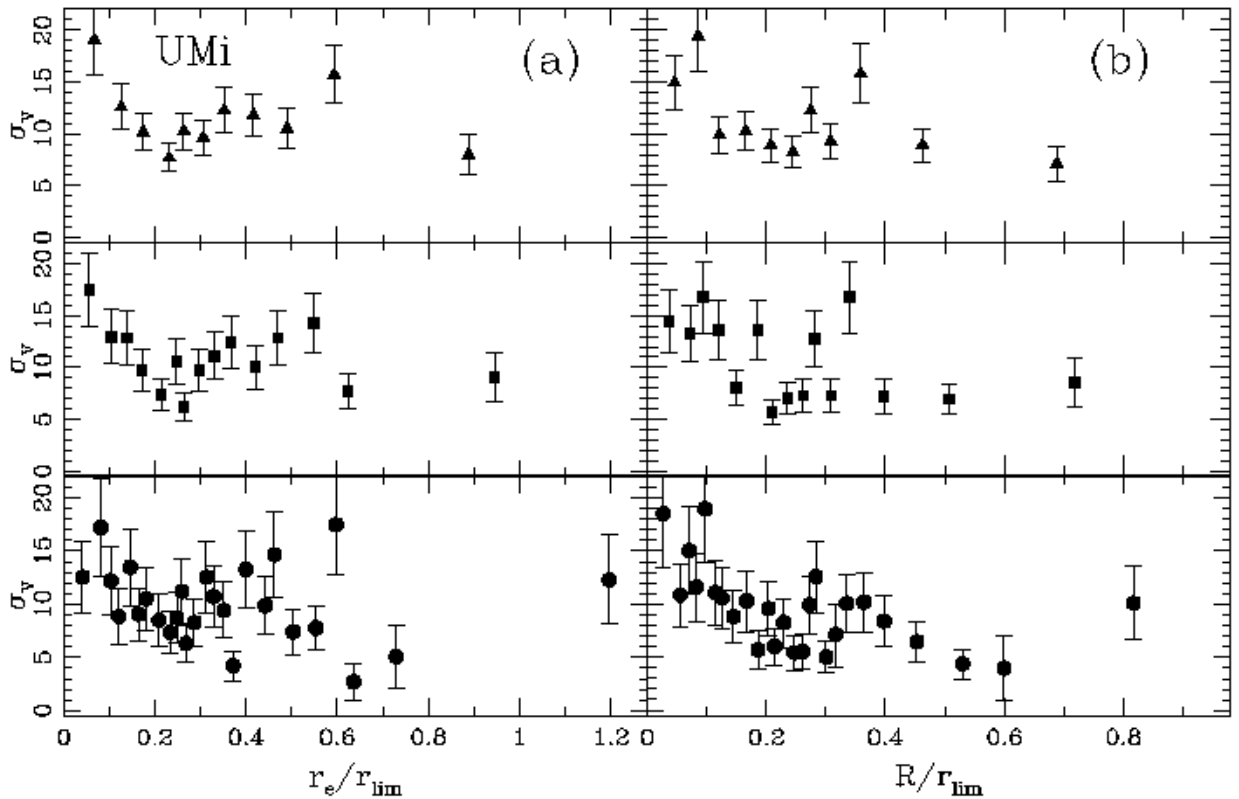


Fig. 3.— RV dispersion profiles for the UMi dSph. From top to bottom, the profiles use 17, 12 and 7 stars per bin respectively. Solid symbols show σ_v 's calculated from the 182 star sample. Panels show profiles versus (a) elliptical and (b) circular radii.

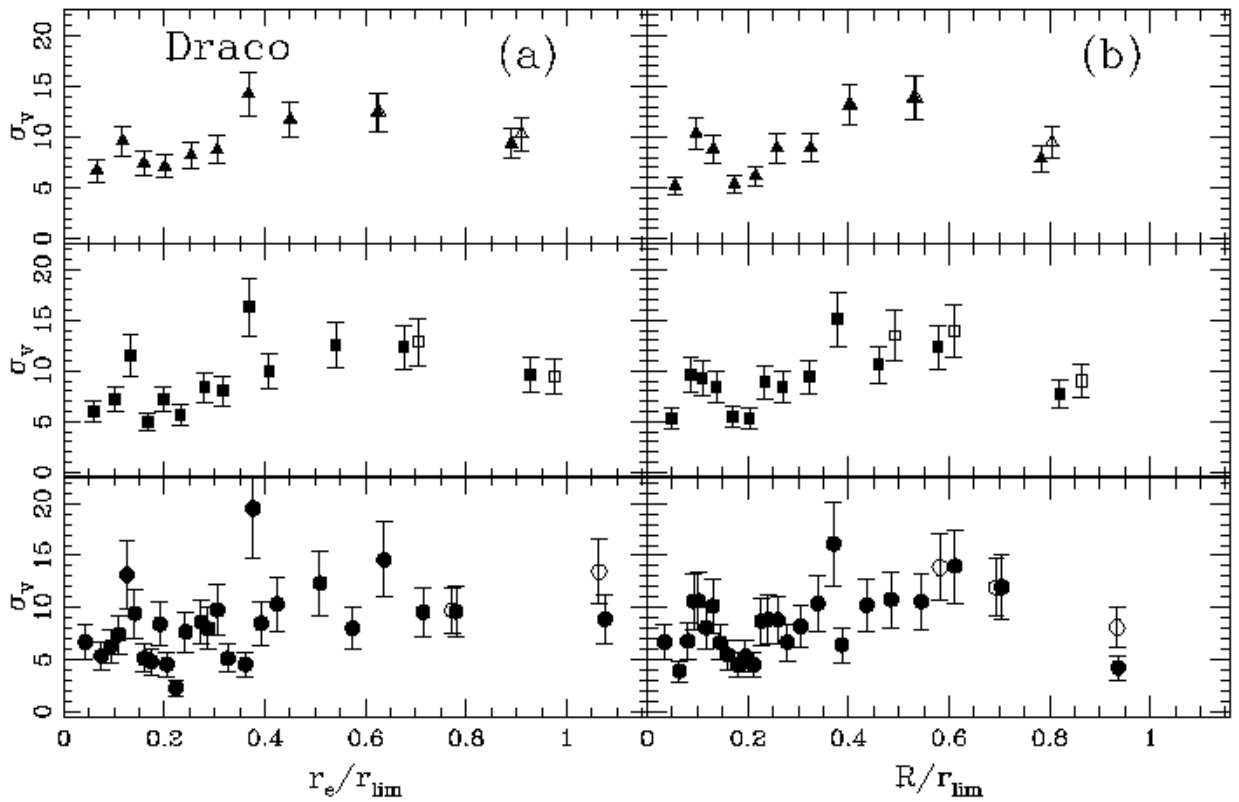


Fig. 4.— Same as Fig. 3 for the Dra dSph. From upper to lower panel, 21, 16 and 8 stars are used per bin, respectively. Open symbols show the profile when the 210 star sample is used.